Available online at www.sciencedirect.com
SCIENCE DIRECT
Nuclear Instruments and Methods in Physics Research A 563 (2006) 268–273
NUCLEAR INSTRUMENTS & METHODS IN PHYSICS RESEARCH Section A
www.elsevier.com/locate/nima

Hard X- and γ-ray measurements with a $3 \times 3 \times 2\,mm^3$ CdZnTe detector

Alan Owens[a,*], T. Buslaps[b], C. Erd[a], H. Graafsma[b], D. Lumb[a], E. Welter[c]

[a]*Science Payload and Advanced Concepts Office, ESA/ESTEC, Postbus 299, 2200AG Noordwijk, The Netherlands*
[b]*Experimental Division, ESRF, Avenue des Martyrs, 38043 Grenoble, Cedex France*
[c]*HASYLAB at DESY, Notkestrasse 85, D 22607 Hamburg, Germany*

Available online 17 February 2006

Abstract

We report the results of a series of X- and γ-ray measurements on a $3 \times 3\,mm^2$, 2 mm thick CdZnTe detector carried out at the HASYLAB and ESRF synchrotron radiation facilities. The detector energy response function was found to be linear over the energy range 10–100 keV with an average rms non-linearity of 0.6%, consistent with statistics. Under full area illumination, the FWHM energy resolution was 270 eV at 5.9 keV and rises to 930 eV at 59.54 keV. Under pencil beam illumination, the measured energy resolution at 10 keV was 310 eV FWHM and rises to ~1000 eV at 100 keV. At 60 keV the resolution was found to be ~30% lower than that measured under uniform illumination, indicating a degree of non-uniform crystallinity and stoichiometry in the bulk. For energies <50 keV, the measured energy-loss spectra show symmetric photopeaks, becoming increasing tailed at higher energies due to hole trapping. Using risetime discrimination (RTD) to filter out events due to holes, it was found that the shape of the photopeaks could be substantially improved at high energies, albeit at the expense of photopeak efficiency. In fact, the relative number of counts in photopeak, dropped from ~90% at 10 keV to ~15% at 100 keV. The results show that a combination of low-noise front-end architecture and RTD leads to very good performances below, say, 100 keV, but above this energy, other techniques (e.g., bi-parametric corrections or single carrier sensing techniques) need to be employed if spectrometric performance is to be maintained.

PACS: 07.85.Nc; 29.30.Kv; 29.40.Wk; 81.05

Keywords: Compound semiconductors; CdZnTe; X-ray detectors; Gamma-ray detectors

1. Introduction

Over the last few decades, there has been considerable interest in the use of compound semiconductors as hard X- and γ-ray photon detectors [1]. Of the available compounds, cadmium zinc telluride (CdZnTe) is probably the most developed and widely used [2]. It has a cubic, zincblende-type lattice structure with atomic numbers close to that of CdTe and a density ~3 times that of Si. CdTe was originally the focus of experimental study in the 1960s, until it was discovered that the addition of a few percent of zinc to the melt results in an increased band gap as well as energy of defect formation. This in turn increases bulk resistivities and reduces the dislocation density, resulting in lower leakage currents. The best spectral performances are achieved with a zinc fraction of ~10%. Typical FWHM energy resolutions at 59.54 keV are in the few keV range at room temperature and decrease with decreasing temperature to a minimum resolution (of $\leqslant 1$ keV) at $\sim -30\,^{\circ}C$ [3].

Although, CdZnTe has many attractive properties it also suffers from some serious drawbacks. For instance, compared to the elemental semiconductors, it has a far high defect density, resulting in a large number of trapping sites. This leads to both uniformity and stability problems and in fact, leakage currents are dominated by these defects rather than the band gap. The large number of trapping sites also ensure that the transport properties of carriers in CdZnTe are far inferior to those of Si and Ge and because of this detector sizes are limited. The problem is exacerbated by the fact that the transport properties of the electrons and holes are markedly different. Typically the mobility-lifetime products of the holes are 10–100 times worse than that of the electrons.

*Corresponding author. Tel.: +31 71 565 5326; fax: +31 71 565 4690.
E-mail address: aowens@rssd.esa.nl (A. Owens).

0168-9002/$ - see front matter © 2006 Elsevier B.V. All rights reserved.
doi:10.1016/j.nima.2006.01.088

In this paper we have carried out a comprehensive characterization of a commercially available CdZnTe detection system making extensive use of both the HASYLAB and ESRF synchrotron research facilities. We instigate its spectral limitations as a function of energy and examine risetime discrimination as an effective method to mitigate the effects of poor hole transport.

2. Detector fabrication

The detector was procured as a complete detection system from Amptek Inc. [4] USA and is based on a $3 \times 3 \times 2\,mm^3$ CdZnTe crystal grown by high-pressure Bridgeman (HPB). The stoichiometric composition was $Cd_{1-x}Zn_xTe$, where $x \approx 0.1$ which results in a band gap energy of 1.572 eV and a density of $5.9\,g\,cm^{-3}$. The detector is mounted on a single stage Peltier element capable of cooling the detector and the input FET of an A250 charge-sensitive preamplifier to $\sim -30\,^{\circ}C$ [5]. Cooling the detector allows higher biases to be applied while cooling the FET increases its transconductance, which reduces the electronic noise of the system. The applied bias was ~600 V. The entire assembly is hermetically sealed in a TO-8 style package. X-rays are viewed through a thin, vacuum tight 250 μm thick Beryllium window.

Since the mobility–lifetime product ($\mu\tau$) of electrons is much greater that that of the holes, negative bias is applied to front electrode to obtain electron collection from the back electrode. This also results in the efficient collection of holes for low incident energies, but poor hole collection at high energies, because of the longer pathlengths they have to traverse. To compensate for this, the system can also make use of inbuilt rise time discrimination (RTD) circuitry, in which only pulses corresponding to full charge collection are selected for further analysis. The rest of the analog chain consists of an Amptek PXT2 spectroscopy amplifier whose output is digitized by an Amptek MCA8000 12-bit ADC and stored on a PC.

3. Experimental

X- and γ-ray experiments were carried out in our laboratory and at the Hamburger synchrotronstrahlungslabor (HASYLAB) radiation facility in Hamburg, Germany, and the European synchrotron research facility (ESRF) in Grenoble, France.

The hard X-ray measurements were carried out on the X1 beamline [6] at HASYLAB. This beamline utilizes a double crystal monochromator to produce highly monochromatic X-ray beams across the energy range 10–100 keV. A Si[5 1 1] reflection was used, yielding an intrinsic energy resolution of ~1 eV at 10 keV rising to 20 eV at 100 keV.

The γ-ray measurements were carried out on the ID15 high-energy scattering beamline [7] at the ESRF. This beamline also utilizes a double crystal monochromator to produce highly collimated photon beams across the energy range 30–1000 keV. A single crystal set was used (Si[3 1 1] reflection). To achieve usable photon fluxes over such an extreme energy range, 2 insertion devices were also used—an asymmetrical multipole wiggler (AMPW) followed by a superconducting wavelength shifter (SCWS). The spectral resolution is typically around 20 eV at 30 keV rising to ~1 keV at 1 MeV.

At both beamlines, the detector was mounted on an X–Y table capable of positioning the detector to a precision of <1 μm in each axis. The beam spot size was set by a pair of precision stepper-driven slits, located immediately in front of the detector. The beam spot size used in most measurements was typically $20 \times 20\,\mu m^2$, normally incident on the detector. For completeness, additional full-area illumination measurements were also carried out using ^{55}Fe and ^{241}Am radioactive sources.

3.1. Measurements

In Fig. 1, we show measured energy-loss spectra from full-area exposures to ^{55}Fe (a) and ^{241}Am (b) with an electronic shaping time of 3 μs. The FWHM energy resolutions of the principal lines at 5.9 and 59.5 keV are 270 and 930 eV FWHM, respectively. The corresponding system noise, as determined by a precision electronic pulser, was 250 eV FWHM. From Fig. 1, we see that the energy resolution is such that the ^{55}Fe Kβ line and the ^{241}Am L-edge sequence of neptunium lines are clearly resolved.

Fig. 2 shows a composite of the detectors response to a series of highly collimated monochromatic spectral lines taken at HASYLAB. The beams were incident at the center of the detector. The detector energy response function was found to be linear over the energy range 10.5–100 keV with an average rms non-linearity of 0.6%, consistent with statistics. Below ~50 keV, the recorded events are confined almost entirely to the photopeaks which are very nearly Gaussian and the level of continuum is extremely low, being $<1\%$ of the photopeak amplitude. Above ~50 keV, the photopeaks become increasingly tailed due to hole trapping. Additionally, the Te and Cd K-edge escape peaks begin to become apparent in the spectrum at energies of 26.7 and 31.8 keV below the photopeaks. The noise floor, which we define to be the lowest energy for which the low energy noise attains an amplitude of 0.5 of the photopeak, occurs at ~0.5 keV.

In Fig. 3, we show the high-energy response measured at the ESRF, for which the deleterious effects of charge trapping are much more apparent. Above about 100 keV, the photopeaks become increasingly tailed and by ~600 keV, no photopeak can be discerned in the energy-loss spectrum. In fact, because of the spectral distortion induced by trapping, the measured energy resolution ceases to increase as a power law with energy, but begins to increase exponentially above ~100 keV (see Section 3.2). In addition, a strong low energy continuum of partial energy

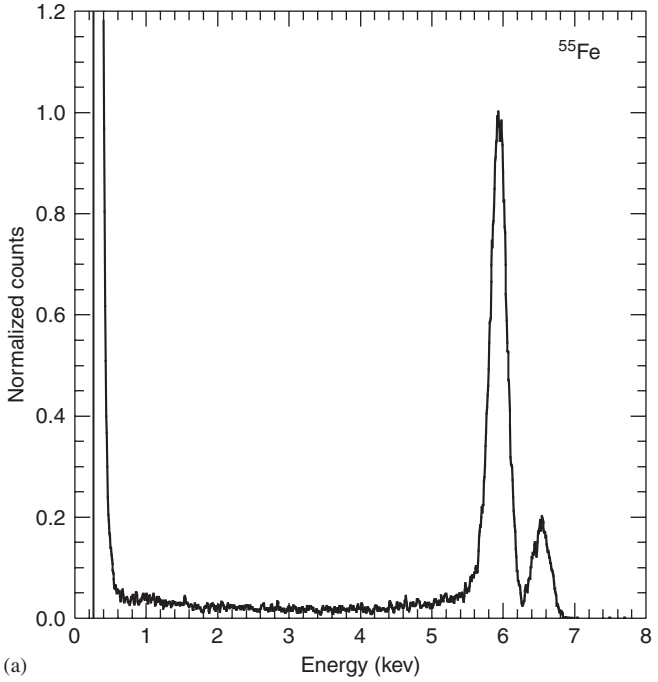

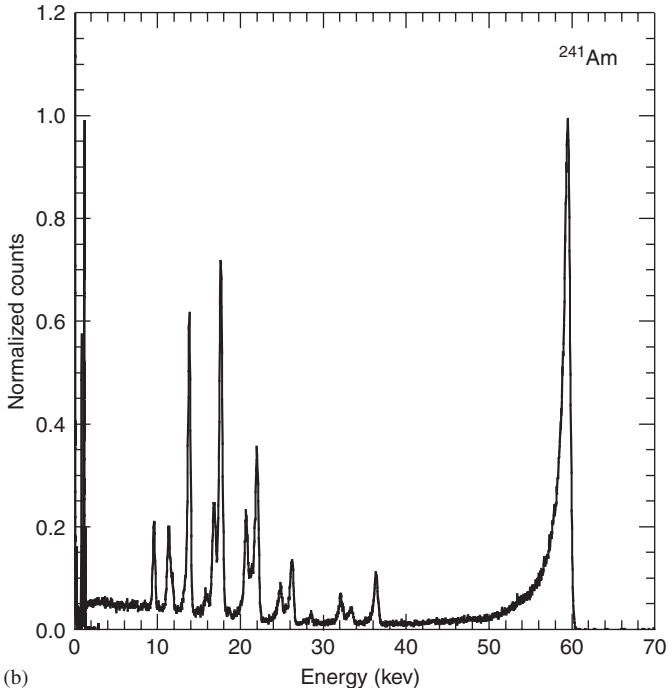

Fig. 1. The measured response of a $3 \times 3 \times 2\,mm^3$ thick CdZnTe detector to: (a) ^{55}Fe and (b) ^{241}Am under full-area illumination.

loss events becomes apparent near ~50 keV, whose amplitude increases rapidly with incident energy.

The energy resolutions determined from Fig. 2 range from 310 eV FWHM at 10 keV to 1.2 keV FWHM at 100 keV and are shown in Fig. 4. The electronic noise of the system, as measured by a precision electronic pulser, was 250 eV FWHM. For the ESRF data, measured FWHM energy resolutions range from ~1.6 keV at 100 keV to 30 keV at 500 keV.

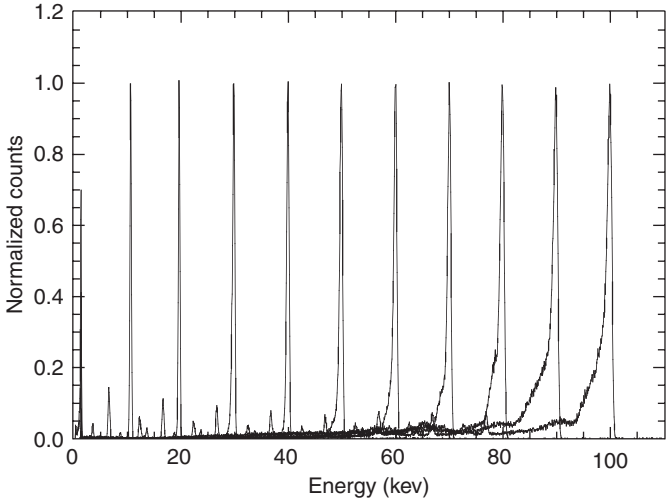

Fig. 2. Composite pulse height spectra of monoenergetic lines measured at HASYLAB. The beam size was $20 \times 20\,\mu m^2$, incident at the center of the detector.

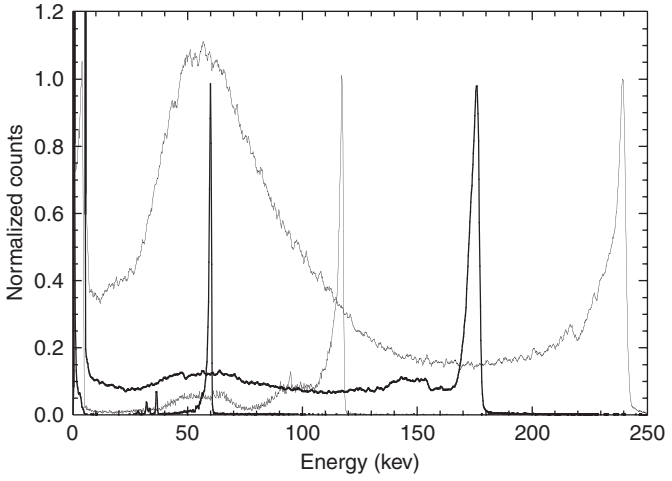

Fig. 3. Composite pulse height spectra of monoenergetic lines measured at the ESRF. The beam size was $20 \times 20\,\mu m^2$, incident at the center of the detector.

3.2. Evaluation of the resolution function

The energy resolution, ΔE, of the system can be described by convolution of probability distributions of three noise components, i.e.,

$$\Delta E = f(\sigma_F^2, \sigma_e^2, \sigma_c^2) \quad (1)$$

where σ_F^2 is the variance of the noise due to carrier generation or Fano noise, σ_e^2 is the variance of the noise due to the leakage current and amplifier noise, and σ_c^2 is the variance of the noise due to incomplete charge collection due to carrier trapping. The contribution due to Fano noise, ΔE_F, was calculated from $\sigma_F^2 = FE\varepsilon$, where F is the Fano factor, ε is the energy to create an electron–hole pair and E is the incident energy. The functional form of ΔE_c is

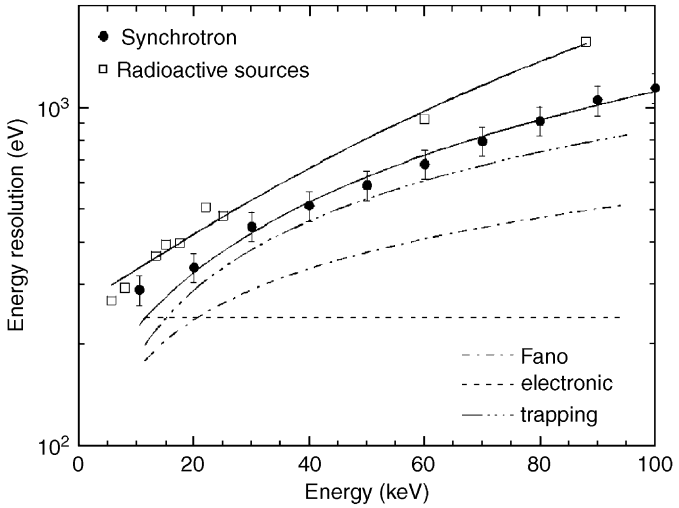

Fig. 4. The energy resolution ΔE measured using a $20 \times 20\,\mu m^2$ pencil beam illumination. The solid line shows the best-fit resolution function to the data. The individual components to the FWHM are also shown for this curve. These are: the noise due to carrier generation, or Fano noise, ΔE_F, electronic noise due to leakage current and amplifier shot noise, ΔE_e, and incomplete charge collection or trapping noise, ΔE_c. For completeness, we also show the measured FWHM energy resolution using full-area illumination with radioactive sources.

assumed to follow the form $\Delta E_c = a_1 E^{a_2}$ [8] where a_1 and a_2 are empirical constants determined by best fitting. Similarly, since the Fano factor is not accurately known, it was also treated as an empirically determined parameter. Assuming all components are normally distributed the resolution function can be described by

$$\Delta E = 2.355\sqrt{F\varepsilon E + (\Delta E_e/2.355)^2 + a_1 E^{a_2}}. \quad (2)$$

Here F, a_1 and a_2 are semi-empirical constants determined by best fitting. The electronic noise component, ΔE_e, was directly measured and fixed at a value of 240 eV FWHM. The best-fit resolution curve and the individual noise contributions to the FWHM (i.e., ΔE_F, ΔE_e and ΔE_c) are shown in Fig. 4. From the figure, we see that electronic noise dominates at energies below 10 keV, while trapping noise dominates above. For completeness, we also show energy resolutions measured under full-area illumination, from which it can be seen that the corresponding resolutions are consistently broader than that measured using pencil beams, indicating a degree of non-uniform crystallinity and stoichiometry in the bulk.

3.3. Risetime discrimination

The PXT2 amplifier also includes switchable risetime discrimination circuitry (RTD) which can be used to compensate for spectral distortion due to charge trapping. RTD is a relatively simple method [9], which relies on the fact that for widely different transport properties, risetimes of the current pulses due to electrons and holes are quite different.

The times taken for an electron and a hole to traverse a detector of width L are

$$t_e = \frac{L}{\mu_e E} \quad \text{and} \quad t_h = \frac{L}{\mu_h E}. \quad (3)$$

In the absence of trapping, the induced signal will build up linearly to the value of the initial charge Q_0, at a rate depending primarily on the carrier with the slowest drift velocity, since by definition, $v_d = \mu E$. The current pulse begins when the carriers induce charge on the electrodes. Given the difference in carrier mobilities, there will clearly be two distinct current pulses, one from holes and one from electrons:

$$I_{h0} = Q_0\left(\frac{\mu_h E}{L}\right) \quad \text{and} \quad I_{e0} = Q_0\left(\frac{\mu_e E}{L}\right). \quad (4)$$

We note from Eqs. (3) and (4), that for the case when $\mu_e \gg \mu_h$ (which is generally true), the current pulse induced by the electrons will have a much larger amplitude and shorter duration than that induced by the holes. For interactions in the bulk of the detector, the induced signal will be a composite of electron and hole components whose relative strengths will now depend on the depth of the interaction. In RTD methods, all pulses whose risetime exceeds a pre-set threshold are rejected—in fact, those events would normally lie in the tail.

The effect of risetime discrimination (RTD) is demonstrated in Fig. 5, in which we show the measured response of the detector to an ^{241}Am source under full area illumination. While the resolution is improved (from 1 keV FWHM at 59.54 keV to 700 eV) using RTD, the efficiency is lower than that expected from the physical dimensions of the detector, since many counts are rejected. This is demonstrated in Fig. 5 in which we can see that the amplitude of the lowest peak at ~9 keV is essentially the

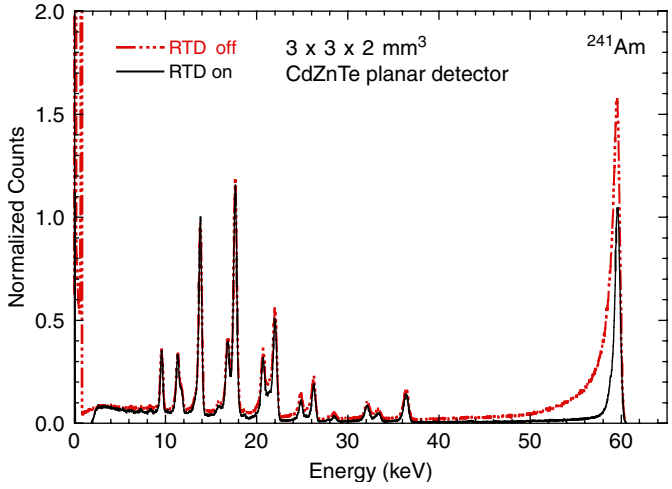

Fig. 5. Two ^{241}Am spectra taken with a $3 \times 3 \times 2\,mm^3$ CdZnTe detector, illustrating the effectiveness of risetime discrimination. From the figure, we see that the hole tailing is substantially reduced when RTD is used and in fact the FWHM energy resolution improves from ~1 keV to 700 eV at 59.54 keV. However, an energy-dependent decrease in photopeak efficiency is also apparent.

same in both spectra, since the entire signal is due to the electrons. However, there is an increasing loss of counts in subsequent peaks of the RTD on spectrum as the energy increases. In fact, at 60 keV the ratio of counts in the photopeak (i.e., RTD-on/RTD-off) is ~0.35 and the ratio of peak heights is ~0.65. In Fig. 6, we show the effect of RTD on high-energy spectra measured using a $20 \times 20\,\mu m^2$ pencil beam at the ESRF. The solid curves show the spectra with RTD and the dotted curves the corresponding spectra without RTD. Although, the results look quite dramatic, it should be noted that each pair of spectra have been normalized so that the height of the photopeaks are the same. In fact at the higher energies, over 90% of events are rejected and the photopeak becomes an increasingly small component of the overall energy-loss spectra. In Fig. 7, we plot the ratio of the counts in the photopeak, both with and without the risetime discrimination switched on illustrating the loss of efficiency when the RTD is switched in. This ranges from ~0.9 at 10 keV to <0.2 at 100 keV. At higher energies, the efficacy of employing RTD is academic, since the primary interaction efficiencies become so low that one might reasonably argue that the detector is entirely unsuitable for γ-ray detection.

Lastly, the effect of risetime discrimination on energy resolution has been evaluated at both HASYLAB and the ESRF using pencil beam illumination. The results are shown in Fig. 8(a) for low energies and Fig. 8(b) for high energies. From Fig. 8(a) we see that for this particular detector, RTD only benefits the energy resolution for incident energies above ~30 keV and slowly improves it with energy (by as much as ~30% at 100 keV). Above ~100 keV, the ratio of resolutions become very nearly constant; viz (FWHM-RTD-off)/(FWHM-RTD-on) = ~0.7.

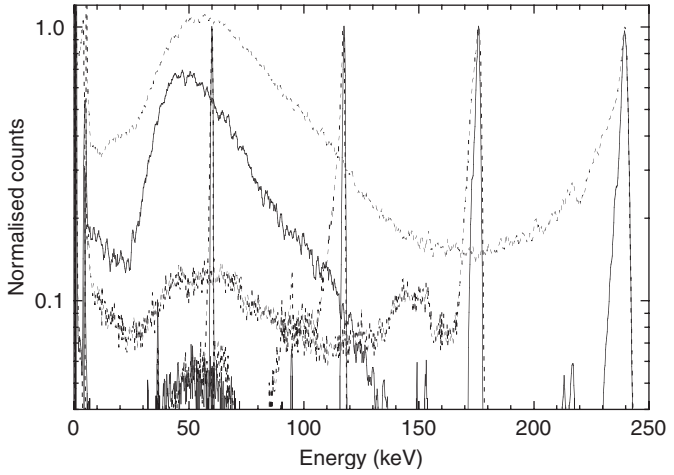

Fig. 6. A composite of energy spectra measured at the ESRF using pencil beam illumination with risetime discrimination switched in (solid curves) and switched out (dotted curves).

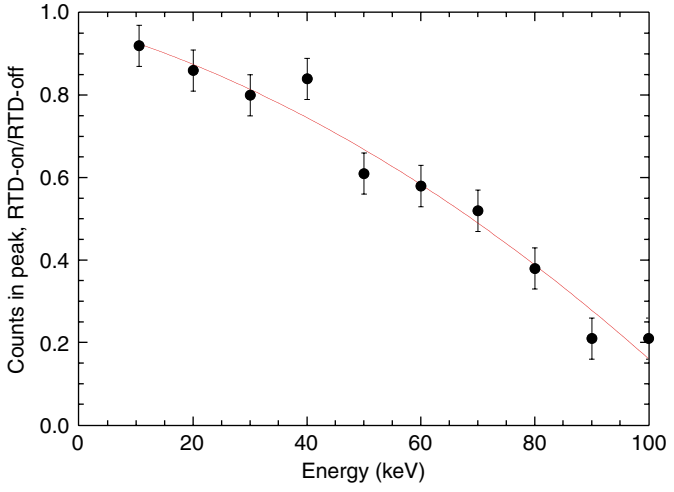

Fig. 7. The ratio of the counts in the photopeak, measured with and without the risetime discrimination (RTD) illustrating the loss of relative efficiency when RTD is employed.

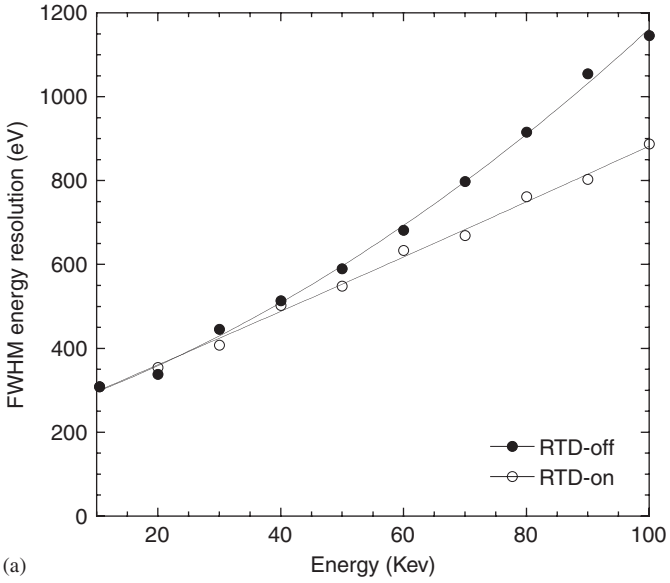

(a)

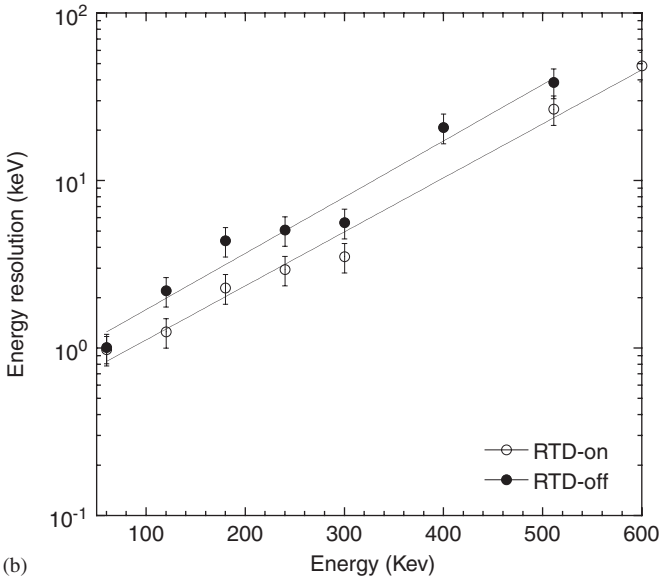

(b)

Fig. 8. The measured FWHM energy resolution as function of energy with the RTD switched on and switched off: (a) low energies measured at HASYLAB and (b) high energies measured at the ESRF.

4. Discussion and conclusions

The present results show that for soft and hard X-ray wavelengths, the present generation of CdZnTe detectors are entirely suitable for most existing and anticipated applications, especially since RTD can provide an effective means for compensating for moderate spectral degradation. For the present system this is applicable for energies below ~100 keV. At higher energies, other techniques, e.g., bi-parametric corrections or single carrier sensing techniques, need to be employed if spectrometric performance is to be maintained.

Acknowledgment

This work was supported by the IHP-Contract II-04-016 EC of the European Commission and by the European Synchrotron Radiation Facility.

References

[1] A. Owens, A. Peacock, Nucl. Instr. and Meth. A 531 (2004) 18.
[2] R. James, T. Schlesinger, J. Lund, M. Schieber, in: T. Schlesinger, R. James (Eds.), Semiconductors for Room Temperature Nuclear Detection Applications, Academic Press, New York, 1995, p. 384.
[3] A. Owens, M. Bavdaz, H. Andersson, T. Gagliardi, M. Krumrey, S. Nenonen, A. Peacock, I. Taylor, Nucl. Instr. and Meth. A 484 (2002) 242.
[4] ⟨http://www.amptek.com/⟩.
[5] R.H. Redus, A.C. Huber, J.A. Pantazis, Nucl. Instr. and Meth. A 458 (2001) 214.
[6] ⟨http://www-hasylab.desy.de/facility/⟩.
[7] ⟨http://www.esrf.fr/UsersAndScience/Experiments/MaterialsScience/ID15/⟩.
[8] A. Kozorezov, J. Wigmore, A. Owens, R. den Hartog, A. Peacock, H.A. Al-Jawhari, Nucl. Instr. and Meth. A 546 (2005) 209.
[9] V.T. Jordanov, J.A. Pantazis, A.C. Huber, Nucl. Instr. and Meth. A 380 (1996) 353.